



Cite this: *Analyst*, 2015, **140**, 7896

Received 22nd June 2015,
Accepted 2nd October 2015

DOI: 10.1039/c5an01240f

www.rsc.org/analyst

Label-free biosensors based on *in situ* formed and functionalized microwires in microfluidic devices†

Yanlong Xing,^{a,b} Andreas Wyss,^c Norbert Esser^d and Petra S. Dittrich^{*‡a}

Label-free biosensors based on *in situ* formed and functionalized TTF–Au wires were developed using an integrated microfluidic system. By applying different modification protocols, TTF–Au wires were successfully used for sensitive label-free detection of catecholamines and human IgG by Raman spectroscopy.

Introduction

The label-free sensing of small molecules and proteins is of high interest for chemical gas and pH sensing, medical diagnostics, and pharmaceutical and biological applications.¹ Novel tools for biosensing have been developed in recent years, among them very promising one-dimensional (1D) nanostructures, *i.e.* fibres, wires and tubes, with the goal to implement them as sensing elements in an operating device. Although experimentally difficult to realize, it is indeed an intriguing outlook that only a single nanostructure is needed for the building of extraordinary small and portable instruments. In particular when combined with microfluidic techniques, 1D-nanostructure sensors can reveal their full potential for the analysis of biological processes and multiplexing for parallel analyses of different target compounds. Microfluidic devices allow the formation, alignment, positioning and immobilization of nano- and micro-sized fibres, while at the same time the fluidic channels could be used as a delivery system to supply analytes to the sensing structures.² One of the intriguing prospects is the integrated synthesis of 1D structures and their final use in sensing applications on a single microfluidic device, making any nano-/microstructure manual handling or micromanipulation unnecessary.^{3–5}

In the past few years, various materials have been utilized to form 1D structures for sensing purposes. For example, crystalline metal oxide nanowires like ZnO or SnO₂ are prepared⁶ and used as capable building elements for conductometric gas

sensors. More difficult is the creation of a sensor for biomolecules, which are dissolved in aqueous solution as, *e.g.*, special care is required for immobilization of the wires. Silicon nanowires, which can be prepared as p- or n-type materials and configured as field effect transistor (FET) based sensor devices, have been utilized to detect biomolecules such as DNA, ATP and proteins.⁷ In this context, semiconducting single walled carbon nanotubes should also be mentioned as they have also been successfully implemented into devices for sensing biomolecules in solution.^{8,9}

Alternatively, hybrid systems created from metal salts and organic compounds have attracted a lot of attention, and were used for building nanodevices.¹⁰ Tetrathiafulvalene–gold (TTF–Au) is a conductive metal–organic hybrid structure and can be formed in a controlled way by using microfluidic-based technology.¹¹ We reported recently on the use of the wires for sensing of water based on conductivity,⁴ and the sensing of vapours of polar organic solvents was also observed (unpublished work). In addition, we also showed the enhancement of the TTF Raman signal on TTF–Au wires.¹² Based on these results, we propose the possibility of using the wires as sensing elements, with conductivity measurements for fast and online readout, and Raman spectroscopy for further identification of the detected molecules. However, to broaden the use of the wires for the detection of a wide range of analytes, several challenges have to be overcome including a method to position and functionalize the wires.

In this study, for the first time, we show the integration of several processes, (i) the bottom-up formation of TTF–Au wires, (ii) the on-chip functionalization of single or a few TTF–Au wires, with different molecules¹³ that have the ability to interact with gold, and (iii) the straightforward use of these wires in biosensing applications. These wires have diameters of a few hundred nanometers up to a few micrometers. To demonstrate that the integrated system is versatile for biological analysis, we have shown selective label-free sensing of catecholamines or human immunoglobulin G (IgG) by applying different modification approaches. The first one enables the

^aDepartment of Chemistry and Applied Biosciences, ETH Zürich, Switzerland.
E-mail: petra.dittrich@bsse.ethz.ch

^bSALSA graduate school, Humboldt-Universität zu Berlin, Germany

^cLaboratory for Nanometallurgy, Department of Materials, ETH Zürich, Switzerland

^dLeibniz-Institute for Analytical Sciences, ISAS Berlin, Germany

† Electronic supplementary information (ESI) available: Experimental details, supplementary figures and movies. See DOI: 10.1039/c5an01240f

‡ Current address: Department of Biosystems Sciences and Engineering, Switzerland.

direct sensing of catecholamines by confocal Raman spectroscopy and is based on wire functionalization by cysteamine (CEA) and glutaraldehyde (GA). The second one enables indirect sensing¹⁴ by using the Raman tag 4-aminothiophenol (4-ATPh).¹⁵ Here, an immunoassay is employed, where the antibody is bound to 4-ATPh and captures the target molecules (human IgG). In addition, the experimental method presented here can be seen as a general means for the functionalization of 1D nano- and microstructures by single- or multi-step reactions.

Experimental section

Chip design

The microfluidic chips were based on the open donut chip design of our group.¹⁶ We used multilayer microfluidic chips made of PDMS by soft lithography, with a fluid layer and a control layer, separated by a thin and flexible PDMS membrane. One chip has six open donuts (diameters 50–250 μm) in the control layer (Fig. 1B), the other one which has eight open donuts with small diameters of 50 and 100 μm (Fig. S4, ESI†) was used for comparison.

TTF–Au *in situ* formation and functionalization

TTF–Au wires were synthesized either by injecting the two solutions (TTF 24 mM, HAuCl₃ 6 mM, both in CH₃CN) with a pipette into the microfluidic chip from either side, or by diffusing a HAuCl₃ solution (6 mM) into the microchannel filled with a TTF solution (24 mM). Here, mainly the diffusion technique was applied. Afterwards, the control layer was pressurized to 3 bar by using N₂ gas to trap the wires formed in the fluid layer. Non-trapped wires were washed away with a solvent. Afterwards, different solutions were supplied at low flow rates (2 to 10 $\mu\text{L min}^{-1}$) into the microchannel, in order to avoid the flow forces to remove the structures. Also, air

bubbles should be carefully avoided to keep the biomolecules, particularly the antibodies, functional during the experiments. We do not recover the wires after the experiment. By using our microchips, the wires could be easily flushed away, just by releasing the pressure on the control layer and washing with a solvent. Afterwards, new wires could be easily formed for further experiment by supplying new TTF and gold solutions into the channel.

Biosensor

Dopamine (DA) hydrochloride was dissolved in an ethanol/PBS 1 : 1 solvent mixture (pH 7.2, PBS final concentration 10 mM) and diluted to concentrations of 5 μM , 15 μM , 25 μM , 35 μM , 50 μM , 75 μM and 100 μM . In this experiment, the solvent mixture ethanol/PBS (1 : 1, pH 7.2) was used unless otherwise stated. CEA solution (10 mM) was firstly supplied into the channel (5 $\mu\text{L min}^{-1}$ for 15 min), then the flow was stopped for 15 min. After washing away excess CEA, a GA solution (5% v/v) was supplied into the channel (2 $\mu\text{L min}^{-1}$ for 20 min) and subsequently washed. Then, different concentrations of DA solutions were pumped into the channel (2 $\mu\text{L min}^{-1}$ for 20 min). After removal of excess DA and subsequent incubation with sodium cyanoborohydride (NaBH₃CN, 1 mM, 2 $\mu\text{L min}^{-1}$ for 15 min), the microchip was washed with PBS buffer (5 $\mu\text{L min}^{-1}$ for 5 min) and then directly used for the Raman measurement.

In addition, the modifications were proven by means of fluorescence microscopy. Generally, a Lissamine rhodamine B sulfonylchloride solution (100 μM , 5 $\mu\text{L min}^{-1}$ for 10 min) was used followed by CEA incubation. After the removal of excess Lissamine rhodamine B sulfonyl chloride using the solvent mixture (5 $\mu\text{L min}^{-1}$, 15 min), fluorescence images were obtained upon excitation with green light. On another chip, 6-aminofluorescein (100 μM) and NaBH₃CN (1 mM) solutions were used successively after supplying GA. The samples without the GA treatment were exposed to 6-aminofluorescein and NaBH₃CN solutions as a negative control. Blue light and appropriate optical filters were used for obtaining fluorescence images.

DL-Norepinephrine hydrochloride, L-epinephrine, isoprenaline hydrochloride, L-phenylalanine and L-tyrosine were dissolved in the solvent mixture to a concentration of 100 μM separately. The functionalization procedures are the same as those applied for DA.

Immunosensor

A DMSO/PBS 2 : 3 solvent mixture (PBS final concentration 10 mM) was prepared and the pH value was adjusted to 7.2. This solution was used as a solvent unless otherwise stated. The antigen (human IgG protein) was dissolved in the solvent mixture and diluted into 5 nM, 10 nM, 30 nM, 50 nM and 70 nM. 4-ATPh (15 mM in CH₃CN) was supplied into the channel at a flow rate of 5 $\mu\text{L min}^{-1}$ for 15 min, then the flow was stopped and the reaction was maintained for another 15 min. At the same time, anti-human IgG antibody (20 $\mu\text{g mL}^{-1}$ in 10 mM PBS buffer, pH 7.4) was incubated in a 1 mL tube with

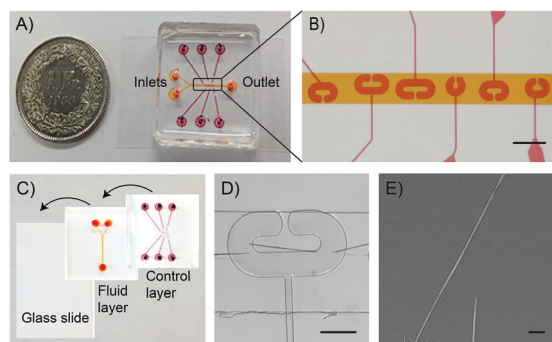


Fig. 1 (A) Photograph of the microdevice with two layers, the control layer in dark red and the fluid layer in orange. (B) A micrograph of the micro-channel and open-donuts. Scale bars: 300 μm . (C) Schematic of the fabrication of the chip. (D) A wire formed inside the donut (scale bar: 100 μm) and (E) SEM image of TTF–Au wires synthesized by diffusion on a non-bonded chip. In this case the long wire is approx. 2 μm wide and 110 μm in length. Scale bar: 10 μm .

1-ethyl-3-(3-dimethylaminopropyl)carbodiimide (EDC, 100 mM in PBS) and *N*-hydroxysuccinimide (NHS, 25 mM in DMSO) for 1 h. After washing off non-reacted 4-ATPh with CH₃CN (10 μL min⁻¹ for 10 min) and the solvent mixture (5 μL min⁻¹ for 10 min), the structures inside donuts were incubated with an antibody solution for 30 min by pipette diffusion. Then, the solvent mixture was used to wash non-bonded antibodies (5 μL min⁻¹ for 10 min). After incubation with CEA (10 mM) as a blocking reagent, different concentrations of antigen (human IgG protein) solutions were supplied into the channel by pipette diffusion and incubated for 20 min. After washing away the excess antigen using PBS buffer (5 μL min⁻¹ for 10 min), the chip was applied for *in situ* Raman measurements.

As in the case of the biosensor, fluorescence microscopy was also employed to prove the wire modifications. Lissamine rhodamine B (100 μM) was used after the incubation of 4-ATPh. Besides, the FITC-labeled human IgG antibody (20 μg mL⁻¹ in PBS buffer, pH 7.4) was first incubated in a 1 mL tube with EDC (100 mM, in PBS) and NHS (25 mM in DMSO) for 1 h, then supplied into the micro-channel by pipette diffusion for 30 min. After washing away surplus FITC-labeled human IgG antibody with PBS buffer (5 μL min⁻¹ for 10 min), fluorescence images were obtained under blue light excitation.

Raman measurement

Raman spectra were recorded on a confocal Raman microscope (CRM 200, WITec GmbH, Germany, Nd:YAG laser, 532 nm) using an upright 100× objective (Nikon, Japan) with a numerical aperture (NA) of 0.9. The laser power was 1.4 mW, and the accumulation time was 2 s. In this measurement, all the signals are collected from large TTF–Au wires (diameter, approx. 2 μm), due to the very small laser point (about 400 nm). Raman spectra were obtained from six wires and averaged to represent the Raman results.

Results and discussion

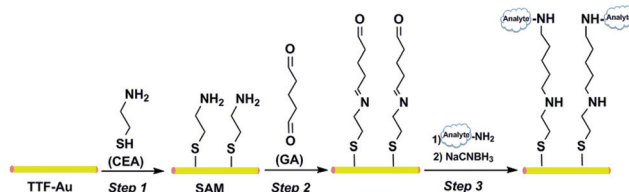
TTF–Au wire formation

TTF–Au wires were formed in a double-layer microchip which has several donut-like features with different diameters and an opening of 25 μm (Fig. 1A–C).¹⁶ This multilayered microfluidic chip combines the ability to synthesize the wires inside the fluid layer channel and the immobilization of wires by pressurizing the control layer with nitrogen gas. There are two advantages in using this chip, firstly the wires trapped in pneumatic cages are not exposed to the shear forces of the fluid flow, and secondly, the fluids can diffuse into the donut traps through the openings, which enable the wires to encounter solutions. In addition, fluids can be easily washed away by using solvents (Movie S1, ESI†). In a typical synthesis of TTF–Au wires, a TTF solution was introduced into the device and afterwards, hydrogen tetrachloroaurate (6 mM in acetonitrile) was added to the inlet reservoirs. The slow diffusion enabled the electron transfer between the two reactants and the fast *in situ* formation of

TTF–Au wires, which were easily monitored on an optical microscope (Fig. 1D and Movie S2, ESI†) and also demonstrated by SEM and energy-dispersive X-ray spectroscopy (Fig. 1E, S3, ESI†). With this diffusion technique, the formed wires were about 2 μm in diameter and varied in length (tens to several hundred micrometers), thus different traps in the control layer were used to immobilize different lengths of wires. A similar chip with many small diameter traps was analysed as well for trapping of more wires (Fig. S4, ESI†).

Label-free biosensor for catecholamines

Due to the presence of Au(0), TTF–Au wires could be further modified. Here we applied two different wire functionalization protocols. Firstly, to find out whether the TTF–Au wires can be used for the sensitive label-free detection of catecholamines, we applied the modification of the wires as indicated in Scheme 1. Using this method, catecholamines can be covalently bonded to the wire and directly monitored by their Raman signals, *i.e.* the analyte is identified by its Raman spectrum. To confirm the formation of the self-assembled monolayer (SAM) of CEA and the binding of GA, fluorescent probes were added after each step that reacted with the terminal groups of the substrates (Fig. 2, see Fig. S5, ESI† for mechanisms). Generally, Lissamine rhodamine B sulfonylchloride, an amino-active fluorescent compound and 6-aminofluorescein (aldehyde-active) were utilized separately after the wires were trapped on different chips (Fig. S6, ESI†). The fluorescent wires in Fig. 2A demonstrated the reaction between the amino



Scheme 1 Functionalization of the TTF–Au wire for the sensing of amines (RNH₂). Step 1: formation of the CEA self-assembled monolayer (SAM) by the Au–S bond; step 2: binding of GA to form a Schiff base;¹⁷ step 3: (1) binding of analytes with the amino group (analyte–NH₂) and (2) treatment with NaCNBH₃ to form the stable secondary amine.¹⁸

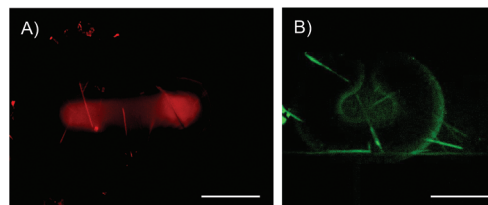


Fig. 2 Fluorescence images of the trapped wires after reaction with (A) 10 mM CEA, 100 μM Lissamine rhodamine B sulfonylchloride, and (B) 10 mM CEA, 5% GA, 100 μM 6-aminofluorescein and 1 mM NaCNBH₃ separately. Scale bars: 100 μm.

groups and Lissamine rhodamine B sulfonylchloride, which proved the formation of SAM of CEA on the wire surface. Similarly, Fig. 2B confirms the reaction between the aldehyde group and 6-aminofluorescein, which proved the successful binding of GA to SAM of CEA. In addition, a control experiment without GA was performed, which showed no fluorescence even after the reaction with 6-aminofluorescein (Fig. S7, ESI†). Next, catecholamines including dopamine (DA), norepinephrine (NE), epinephrine (EPI) and isoprenaline (ISP) (Fig. S8, ESI†) were detected separately by the proposed method. Micro-Raman spectroscopy was performed to acquire signals from every single wire. It has been reported that the TTF-Au wire had a typical Raman peak at around 1426 cm^{-1} .¹² Compared to the spectra of the single TTF-Au wire, two additional Raman peaks at 1268 cm^{-1} and 1476 cm^{-1} appeared after the binding of DA to the modified wire (Fig. S9A, ESI†), which clearly demonstrated the binding of DA to GA.¹⁹ In addition, NE showed similar spectra to DA, with the typical bands at 1268 cm^{-1} and 1479 cm^{-1} ($0\text{--}3\text{ cm}^{-1}$ shifted from the corresponding bands in DA), and a slightly lower intensity than DA (Fig. S9A, ESI†). However, EPI and ISP only yielded very weak Raman bands (Fig. S9A, ESI†), which may be due to their weak Raman intensities.²⁰ To show the selectivity of the system, aromatic amino acids that are related to the formation of neurotransmitters, phenylalanine (Phe) and tyrosine (Tyr) (Fig. S8, ESI†), were also detected for comparison. As expected, Phe and Tyr exhibited totally different Raman bands with DA (Fig. S9B, ESI†). Thus, using the proposed sensor, we can clearly distinguish catecholamines from other bioamines that have Raman bands in the similar range ($1200\text{ cm}^{-1}\text{--}1700\text{ cm}^{-1}$).

Furthermore, quantitative measurements were performed using dopamine, a well-known neurotransmitter.²¹ Although DA has a weak Raman signal,²² we observed obvious changes in the intensity of the Raman response with the increasing concentration from $5\text{ }\mu\text{M}$ to $100\text{ }\mu\text{M}$ (Fig. 3A). Typically, the signal intensity at 1476 cm^{-1} can be used for the quantification of DA. For data analysis, we applied a subtracted baseline to calculate the peak intensity at 1476 cm^{-1} (Fig. S10,

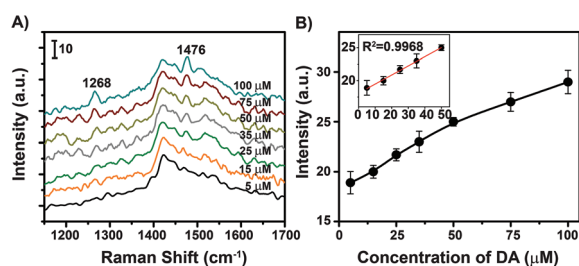
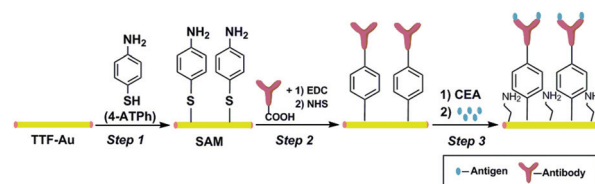


Fig. 3 (A) Representative Raman spectra of the biosensor for increasing concentrations of DA from $5\text{ }\mu\text{M}$ – $100\text{ }\mu\text{M}$. (B) Raman intensity at around 1476 cm^{-1} for different concentrations of DA after data correction. The inset figure shows the linear relationship in the concentration range from $5\text{--}50\text{ }\mu\text{M}$ (coefficient of determination, $R^2 = 0.9968$). Error bars indicate standard deviations from six measurements.

ESI†) that was plotted against the DA concentration. The relationship between Raman intensities and different concentrations at the micromolar level of DA is shown in Fig. 3B. In addition, a linear response was obtained between the Raman intensity and DA in the concentration range from 5 to $50\text{ }\mu\text{M}$ (Fig. 3B inset). The detection limit of this technique ($\sim 15\text{ }\mu\text{M}$) is lower than that of the recently reported method²² ($\sim 100\text{ }\mu\text{M}$) which is also based on the Raman measurement.

Label-free immunosensor for human IgG

Next, to evaluate whether a microfluidic integrated TTF-Au wire system can be used for sensitive label-free immunoassay, we have applied another functionalization protocol and tested it for the detection of human IgG. Here, we used the phenol-based Raman reporter molecule, 4-ATPh, as a linker between the wire and the capture antibody. Former studies proved that 4-ATPh is a nano-mechanical stress sensor that can be employed as an indicator for the binding of antigens to antibodies as the deformation in the stretching mode of the benzene ring upon binding events results in changes in Raman frequencies of 4-ATPh.^{15,23} The Raman shifts correspond to different concentrations of antigens binding to antibodies. Scheme 2 shows the procedure for the functionalization of the wire. As in the label-free sensor for catecholamines (Fig. 2), fluorescently tagged compounds were bound to the wires to demonstrate the formation of the SAM of 4-ATPh and the binding of the antibodies to the wire (see Fig. S11, ESI† for mechanisms). After the immobilization and functionalization of the wires (Fig. S12 ESI†), their fluorescence clearly demonstrated the reaction between Lissamine rhodamine B and the SAM of 4-ATPh (Fig. 4A), as well as the successful binding of pretreated FITC-labelled anti-human IgG antibody (Fig. 4B). Afterwards, the immunoassay of human IgG in combination with the proposed sensor by Raman spectroscopy was performed. Fig. 5A shows the Raman spectra of pure solid 4-ATPh, TTF-Au and the substrate of TTF-Au/4-ATPh. Pure 4-ATPh shows typical peaks at 390 cm^{-1} , 470 cm^{-1} , 1092 cm^{-1} and 1597 cm^{-1} (curve a), and TTF-Au shows characteristic Raman bands at 506 cm^{-1} and 1426 cm^{-1} (curve b). Compared to the spectra of pure 4-ATPh, the absence of the peak at 470 cm^{-1} and the shifts of peaks from 1092 cm^{-1} and 1597 cm^{-1} to 1080 cm^{-1} and 1581 cm^{-1} , respectively, in the spectra of TTF-Au/4-ATPh (curve c) indicate the formation of



Scheme 2 Functionalization of the TTF-Au wire for immunoassay. Step 1: SAM of 4-ATPh; step 2: immobilization of the capturing antibody (anti-human IgG) by using EDC/NHS. Step 3: (1) blocking the unreacted wire surface by CEA and (2) antigen (human IgG) binding.

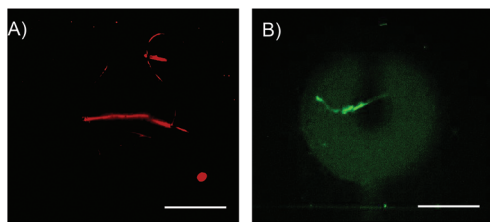


Fig. 4 Fluorescence images of the trapped wires after reaction with (A) 15 mM 4-ATPh and 100 μM Lissamine rhodamine B sulfonylechloride; and (B) 15 mM 4-ATPh and 20 $\mu\text{g mL}^{-1}$ FITC-labeled human IgG antibody (pretreated with EDC/NHS). Scale bars: 100 μm .

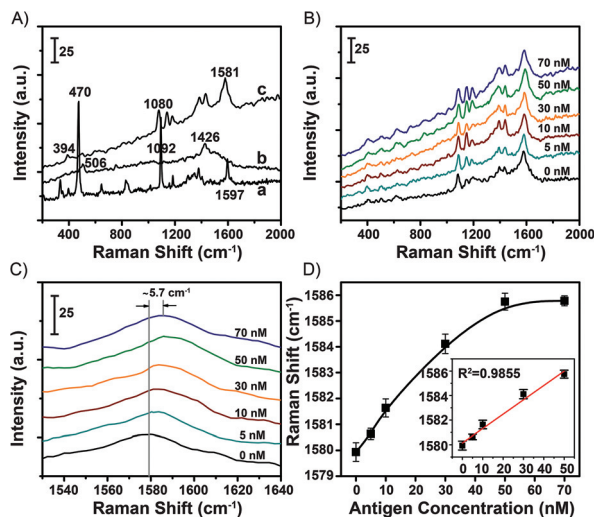


Fig. 5 (A) The Raman spectra of pure 4-ATPh (curve a), TTF-Au wire (curve b) and TTF-Au/4-ATPh (curve c). (B) Representative Raman spectra of the immunosensor in the presence of increasing concentrations of human IgG range from 0 nM to 70 nM. (C) Raman peaks at around 1580 cm^{-1} of the representative spectra of the immunosensor of TTF-Au/4-ATPh/anti-human IgG in the presence of increasing concentrations of human IgG. (D) Corresponding Raman peak shifts to different antigen concentrations. The inset figure shows the linear relationship in the concentration range from 0–50 nM (coefficient of determination, $R^2 = 0.9855$). Error bars indicate standard deviations from six measurements.

the SAM of 4-ATPh on TTF-Au wires.²⁴ The spectra of the antibody-conjugated wire (TTF-Au/4-ATPh/anti-human IgG) incubated with different concentrations of antigen varying from 0 nM to 70 nM are shown in Fig. 5B. The typical Raman peaks around 1580 cm^{-1} , corresponding to the benzene ring stretching of 4-ATPh, are responsive to the antibody-antigen binding.²³ As is clearly visible in the high magnification spectra in Fig. 5C, with an increasing concentration of human IgG ranging from 0 to 70 nM, the Raman frequencies of the sensor shifted to higher wavenumbers for about 5.7 cm^{-1} as expected. Fig. 5D shows the calibration curve of the immunoassay. A good linear response was obtained for an antigen concentration below 50 nM (Fig. 5D inset). The plateau for larger concentrations indicated saturation of the antigen-

antibody complex. This method is very sensitive with a low limit of detection (~ 5 nM).

In our experiment, due to the larger diameter of the wires (approx. 2 μm , Fig. 1E) than the Raman laser point (400 nm), we were sure that all the Raman signals were collected from the structures. Together with the reasonable small error bars obtained from different wires, the reproducibility of the two proposed protocols was also well demonstrated (Fig. 3D and 5D).

Conclusions

In conclusion, we have reported an integrated TTF-Au wire based microfluidic system with a sensitive label-free bio-sensing capability. With this method, the direct sensing of catecholamines involving dopamine and the indirect sensing of human IgG were achieved, both in concentration ranges comparable to the recently reported work, but here on single wires.^{15,22} Due to the similar structures and Raman spectra of dopamine and its carbon-hydroxylated product norepinephrine, the proposed direct sensing method still lacks high selectivity in distinguishing these catecholamines, which is also a limitation of former studies using Raman spectroscopy.²⁵ However, the two approaches reported herein are of general interest for various hybrid structures with active surfaces and open a new way for *in situ* formed micro- and nanowire sensing devices with integrated delivering systems. In the future, by improving the positioning and alignment of the wires inside the microchip, a single micro-/nanowire sensor system can also be fabricated, which is very attractive as advanced sensing tools for chemicals and biomolecules, *e.g.* for single-cell analysis methods.

Acknowledgements

Funding from the Excellence Initiative Deutsche Forschungsgemeinschaft is gratefully acknowledged. We thank the Scientific Center for Optical and Electron Microscopy (ScopeM) of ETH Zürich for their facilities. Great thanks to Klaus Eyer, Dr Tom Robinson and Daniel Bernoulli for their help.

Notes and references

- 1 B. Tian, X. Zheng, T. J. Kempa, Y. Fang, N. Yu, G. Yu, J. Huang and C. M. Lieber, *Nature*, 2007, **449**, 885.
- 2 M. Lee, K. Y. Baik, M. Noah, Y.-K. Kwon, J.-O. Lee and S. Hong, *Lab Chip*, 2009, **9**, 2267.
- 3 S. Hou, S. Wang, Z. T. F. Yu, N. Q. M. Zhu, K. Liu, J. Sun, W.-Y. Lin, C. K. F. Shen, X. Fang and H.-R. Tseng, *Angew. Chem., Int. Ed.*, 2008, **47**, 1072.
- 4 B. Z. Cvetkovic, J. Puigmarti-Luis, D. Schaffhauser, T. Ryll, S. Schmid and P. S. Dittrich, *ACS Nano*, 2013, **7**, 183.
- 5 J. Kim, Z. Li and I. Park, *Lab Chip*, 2011, **11**, 1946.

- 6 E. Comini, C. Baratto, G. Faglia, M. Ferroni, A. Vomiero and G. Sberveglieri, *Prog. Mater. Sci.*, 2009, **54**, 1.
- 7 F. Patolsky, G. Zheng and C. M. Lieber, *Anal. Chem.*, 2006, **78**, 4260.
- 8 R. J. Chen, S. Bangsaruntip, K. A. Drouvalakis, N. Wong Shi Kam, M. Shim, Y. Li, W. Kim, P. J. Utz and H. Dai, *Proc. Natl. Acad. Sci. U. S. A.*, 2003, **100**, 4984.
- 9 K. Besteman, J.-O. Lee, F. G. M. Wiertz, H. A. Heering and C. Dekker, *Nano Lett.*, 2003, **3**, 727.
- 10 W. U. Huynh, J. J. Dittmer and A. P. Alivisatos, *Science*, 2002, **295**, 2425.
- 11 J. Puigmartí-Luis, D. Schaffhauser, B. R. Burg and P. S. Dittrich, *Adv. Mater.*, 2010, **22**, 2255.
- 12 J. Puigmartí-Luis, J. Stadler, D. Schaffhauser, A. P. del Pino, B. R. Burg and P. S. Dittrich, *Nanoscale*, 2011, **3**, 937.
- 13 J. C. Love, L. A. Estroff, J. K. Kriebel, R. G. Nuzzo and G. M. Whitesides, *Chem. Rev.*, 2005, **105**, 1103.
- 14 X. X. Han, L. Chen, W. Ji, Y. Xie, B. Zhao and Y. Ozaki, *Small*, 2011, **7**, 316.
- 15 K. W. Kho, U. S. Dinish, A. Kumar and M. Olivo, *ACS Nano*, 2012, **6**, 4892.
- 16 P. Kuhn, J. Puigmartí-Luis, I. Imaz, D. Maspoch and P. S. Dittrich, *Lab Chip*, 2011, **11**, 753.
- 17 Y. Wang, K. Lee and J. Irudayaraj, *Chem. Commun.*, 2010, **46**, 613.
- 18 A. W. Miller and J. F. Robyt, *Biotechnol. Bioeng.*, 1983, **25**, 2795.
- 19 M. L. Mcglashen, K. L. Davis and M. D. Morris, *Anal. Chem.*, 1990, **62**, 846.
- 20 N. S. Lee, Y. Z. Hsieh, R. F. Paisley and M. D. Morris, *Anal. Chem.*, 1988, **60**, 442.
- 21 L. Sasso, A. Heiskanen, F. Diazzi, M. Dimaki, J. Castillo-Leon, M. Vergani, E. Landini, R. Raiteri, G. Ferrari, M. Carminati, M. Sampietro, W. E. Svendsen and J. Emneus, *Analyst*, 2013, **138**, 3651.
- 22 Y. J. Oh and K. H. Jeong, *Lab Chip*, 2014, **14**, 865.
- 23 J. Perumal, K. V. Kong, U. S. Dinish, R. M. Bakker and M. Olivo, *RSC Adv.*, 2014, **4**, 12995.
- 24 X. G. Hu, T. Wang, L. Wang and S. J. Dong, *J. Phys. Chem.*, 2007, **111**, 6962.
- 25 M. Volkan, D. L. Stokes and T. Vo-Dinh, *Appl. Spectrosc.*, 2000, **54**, 1842.